A&A 399, 51–61 (2003)
DOI: 10.1051/0004-6361:20021784

Astronomy & Astrophysics

GHASP: An Hα kinematic survey of spiral and irregular galaxies⋆

II. Velocity fields and rotation curves of 15 galaxies

O. Garrido, M. Marcelin, P. Amram, and O. Boissin

Observatoire Astronomique Marseille-Provence & Laboratoire d'Astrophysique de Marseille, 2 place Le Verrier, 13248 Marseille Cedex 04, France

Received 8 August 2002 / Accepted 19 November 2002

Abstract. We present Fabry-Perot images obtained during the GHASP survey (Gassendi Hα survey of SPirals). We have derived the Hα maps, the 2D velocity fields and the rotation curves for a new set of 15 galaxies, increasing the sample we plan to build. The majority of the objects studied here are late-type spirals (Sc-Sdm) and irregular galaxies. Only 8 galaxies have a regular and symmetric rotation curve (two of them have a solid-body rotation curve) and they are all of morphological type earlier than 8 ≈ Sd. Five galaxies present an irregular rotation curve and they are all very late-type galaxies ($t \geq 8.8$). For one galaxy, UGC 2053, no rotation curve could be derived, and for another one, UGC 11300, both sides have completely different behaviors. All of them have already been observed in HI by the WHISP survey led at Westerbork, for which GHASP brings an interesting complement.

Key words. galaxies: kinematics and dynamics – galaxies: spiral – galaxies: irregular – galaxies: dwarf

1. Introduction

GHASP (acronym for Gassendi Hα survey of SPirals) is a survey of galaxies at the wavelength of the Hα emission line begun in 1998 at the Observatoire de Haute-Provence. The aim is to obtain high resolution 2D velocity fields in the Hα line of hydrogen for about 200 nearby spiral and irregular galaxies, using a scanning Fabry-Perot interferometer in a focal reducer attached at the Cassegrain focus of the 1.93 m telescope. The accuracy is on average about 5 km s^{-1} (depending of the S/N) in velocity and 2 arcsec in spatial resolution (limited by the average seeing for typical exposures of 2 hours).

The GHASP survey will provide a homogeneous sample of 2D velocity fields which will cover a large range of luminosities (and masses) and morphological types (except for Es and SOs for which Hα emission is several orders of magnitude weaker), providing a complete reference sample at $z = 0$. In order to obtain a self-consistent sample in agreement with the scientific goals and a reasonable number of observing runs for the data acquisition on the telescope, we have estimated that a sample of 200 galaxies has to be observed. Indeed, we expect to cover and sample the plane "galaxy mass - galaxy morphological type". For convenience, we use the plane "luminosity - morphological type" in the ranges: $-16 \leq M_b \leq -23$ and $1 \leq t \leq 10$ (de Vaucouleurs 1979). We have defined bins of 1.4 in magnitude and 2 in morphological type, each bin containing 8 galaxies, leading to a total of 5×5×8 = 200 galaxies. Non-barred galaxies as well as barred galaxies are selected in each bin. Of course, M_b is not the best physical indicator of the total mass of a galaxy (M_R, M_I, M_H are much better) but it is available for a large range of galaxies in the literature(note that the maximum rotational velocity is extracted from the data and remains the best indicator of the total mass, at least within the optical radius).

There is no large and homogeneous sample of 2D velocity fields at optical wavelengths of field galaxies. Most of the Fabry-Perot observations found in the literature are concerned with the study of individual galaxies or small samples (e.g. Plana et al. 2000, showing that the Hickson compact group 18 is in fact a large irregular galaxy with several star-forming clumps; Gavazzi et al. 2001, kinematical study of the complexe edge-on galaxy UGC 6697; Rozas et al. 2002, kinematical observations of the active barred spiral NGC 6951; Garcia-Barreto et al. 2001, study of the kinematical properties of the barred spiral NGC 3367; Östlin et al. 1999, 2001, dynamical study of six luminous blue compact galaxies; Mendes de Oliveira et al. 2001, kinematical study of seven candidate tidal dwarfs in the Stephan's Quintet; Beauvais & Bothun 2001, sample of Fabry-Perot data for seven late-type spiral galaxies). The largest sample obtained up to now is that of 75 galaxies (located in the southern sky) studied by Schommer et al. (1993) to measure galaxy distances (Tully-Fisher relation) and for which Palunas et al. (2000) have applied maximum disk mass models. With this survey, we plan to complement the radio survey WHISP (Westerbork survey of HI in SPirals galaxies) carried out at Westerbork since 1993

Send offprint requests to: O. Garrido,
e-mail: olivia.garrido@oamp.fr

⋆ Based on observations collected at the Observatoire de Haute de Provence.

and providing HI distribution and velocity maps for about 400 galaxies (http://www.astro.rug.nl/~whisp/). The complementarity of GHASP and WHISP has been discussed in Paper I.

2. Observations and data reduction

The instrument principle, characteristics, as well as the description of data processing, are given in Paper I (Garrido et al. 2002). More details can be found on our Web site: http://www-obs.cnrs-mrs.fr/interferometrie/GHASP/ghasp.html. The first set of 23 galaxies, observed in autumn 1998 and spring 1999, has been presented in Garrido et al. (2002, Paper I). Since then, runs have taken place every semester (typically 9 to 13 nights per run). We present here the results of the third run, consisting of 15 galaxies, observed in September 1999; all of them have already been observed by WHISP. In particular two of them, UGC 2023 and UGC 2053, have been studied by Swaters in the context of the WHISP survey (1999).

The data processing has been pushed toward lower thresholds (in terms of Hα emission) than for Paper I. We also reprocessed the original data of Paper I in order to reach fainter and more diffuse Hα emission. The resulting velocity fields are better defined than those originally published in Paper I, since they are based on a larger number of velocity points. Most of these points come from the diffuse Hα emission of the disk for which the signal to noise is significantly lower than in the bright HII regions. The resulting velocity fields and rotation curves (with the new derived kinematical parameters) can be found on the GHASP web site.

Table 1 gives the journal of the observations, with the following information:
(1) name of the galaxy in the UGC catalog;
(2) name in the NGC catalog when available;
(3) and (4) coordinates of the galaxy in 2000;
(5) morphological type from the RC3 catalog;
(6) central wavelength of the interference filter used;
(7) $FWHM$ of the interference filter used for the observation;
(8) date of the observations;
(9) total exposure time in seconds.

Table 2 gives the values we found for the main kinematical parameters, together with some fundamental parameters found in the literature:
(1) name in the UGC catalog;
(2) morphological type code t from the de Vaucouleurs classification (de Vaucouleurs 1979) in the LEDA data base (Lyon-Meudon Extragalactic Database);
(3) total apparent corrected B magnitude, B°_{T}, from LEDA;
(4) absolute B magnitude, $M_{\rm b}$, from LEDA;
(5) systemic velocity deduced from our velocity field;
(6) distance D, deduced from the systemic velocity taken in the NED, assuming $H_{\rm o}$ = 75 km s^{-1} Mpc^{-1};
(7) inclination deduced from the analysis of our velocity field, except for UGC 2023 and 2053 already studied by Swaters (1999) and for which the lack of Hα data makes it difficult to derive the inclination;
(8) position angle of the major axis deduced from our velocity field;
(9) maximal amplitude velocity, $\Delta V_{\rm max}$, observed on the rotation curve (we do not take into account the extremal points in the case of warps);
(10) maximum velocity, $V_{\rm max}$, observed on the rotation curve;
(11) and (12) outermost velocity point reached on the rotation curve, $V_{\rm last}$ and $R_{\rm last}$ being respectively the velocity and distance from the rotation center for this point;
(13) 1/2 S.A. is the half sector around the major axis taken into account for computing the rotation curve.
A detailed discussion of the problem of the systemic velocity is given in Paper I.

3. Reduced Hα data

For each galaxy we give the results of the data reduction in Figs. 1 to 15, with two frames per figure:

a. Isovelocity lines superimposed on the Hα image of the galaxy (a colour coded version of the velocity field is available on the Web site of GHASP). These lines were drawn from the original velocity field (with velocities computed from the original data cube smoothed spatially on 3 × 3 pixels and spectrally on 3 channels) after a strong Gaussian smoothing (7 pixels $FWHM$), sometimes reiterated when the coverage of the galaxy by HII regions is faint, so as to obtain continuous lines. At some places with poor Hα emission the continuity of the lines was artificially achieved by eye estimate and a dashed line plotted on the velocity field. In the worst cases, with only a few isolated HII regions measured in a galaxy, it was impossible to draw any isovelocity line, and we directly wrote the average velocity value found for each HII region on the map. The Hα image is derived from the analysis of the Hα line profiles, by measuring the flux found inside the line for each pixel (each pixel has a size of 0.96 square arcseconds). It gives a pure monochromatic image of the galaxy (continuum-free). The intensity is coded here through gray levels (note we have only relative intensity levels but no absolute calibration). Note that sometimes the Hα images are markedly offcentered; this is the case when we have to shift a bright star out of the field to prevent any damage to the microchannel plate of the IPCS but also when we offcentered the galaxy in order to prevent ghosts (due to ghost reflections inside the instrument between Fabry-Perot plates and interference filter) from contaminating other parts of the galaxy. It must be noted also that in some cases, when the velocity amplitude is high with respect to the width of the interference filter and the interference filter is not centered on the systemic velocity, one side of the galaxy is better transmitted than the other side, leading to an artificial asymmetry in the intensity of the Hα emission. This will be specified in the cases when it occurs.

b. Rotation curve of the galaxy. The rotation curve is drawn as explained in Paper I, using the velocity field obtained after a Gaussian smoothing of 3 pixels $FWHM$. The curve is plotted with both sides superimposed in the same quadrant, using different symbols for the receding and approaching side (with respect to the center itself): crosses are for receding and dots for approaching. To compute the values of the velocity and the

Table 1. Log of the observations.

No. UGC (1)	No. NGC (2)	α (3)	δ (2000) (4)	Type (2000) (5)	λ_c Å (6)	$FWHM$ Å (7)	date (1999) (8)	exposure time (s) (9)
528	278	$00^h52^m04.4^s$	47°33′02″	SAB(rs)b	6577	11	September, 4	4320
1249		$01^h47^m29.9^s$	27°19′59″	SB(s)m	6567	12	September, 14	5280
1256	672	$01^h47^m54.3^s$	27°25′59″	SB(s)cd	6577	11	September, 10 and 11	13 200
2023		$02^h33^m18.2^s$	33°29′28″	Im	6577	11	September, 8	5520
2053		$02^h34^m29.3^s$	29°44′59″	Im	6587	11	September, 5 and 7	11 760
2082		$02^h36^m16.1^s$	25°25′27″	Sc	6577	11	September, 12	7200
2855		$03^h48^m20.6^s$	70°07′59″	SABc	6587	11	September, 13	7200
10 897	6412	$17^h29^m37.5^s$	75°42′16″	S(s)c	6597	10	September, 12	7200
11 218	6643	$18^h19^m46.6^s$	74°34′10″	S(rs)c	6597	10	September, 9	7200
11 283		$18^h33^m52.6^s$	49°16′43″	SB(s)dm	6606	12	September, 7 and 10	9600
11 283c		$18^h34^m01.0^s$	49°22′15″	?	6606	12	September, 5	7200
11 300	6689/90	$18^h34^m50.1^s$	70°31′27″	SBcd	6577	11	September, 11	7200
11 891		$22^h03^m33.9^s$	43°44′57″	Im	6577	11	September, 4	10 800
11 951	7231	$22^h12^m30.1^s$	45°19′42″	SBa	6587	11	September, 6	7200
12 212		$22^h50^m30.3^s$	29°08′18″	Sm	6587	11	September, 9 and 13	13 440

Table 2. Galaxy parameters.

No. UGC (1)	t (2)	B°_T (mag) (3)	M_b (mag) (4)	V_{sys} (km s^{-1}) (5)	D (Mpc) (6)	i (°) (7)	PA (8)	ΔV_{max} (9)	V_{max} (km s^{-1}) (10)	V_{last} (km s^{-1}) (11)	R_{last} (″) (12)	1/2 S.A.(°) (13)
528	2.9	10.8	−19.4	626.5 ± 1	6.3	25 ± 10	219 ± 1	148 ± 6	83 ± 1	+83 ± 1	+38	50
1249	8.9	11		345 ± 1	4.5	60 ± 8	319 ± 1	161 ± 6	81 ± 7	−71 ± 10	−174	40
1256	6	10.5	−19.6	422 ± 2	5.6	65 ± 3	244 ± 3	199 ± 1	100 ± 5	−96 ± 6	−160	40
2023	9.9	13.5	−16.4	589 ± 1	8	19 ± 5	134 ± 2	139 ± 8	87 ± 19	+60 ± 5	+77	50
2053	9.9	14	−16.9		14							
2082	5.8	11.6	−18.5	696 ± 1	9.3	80 ± 2	127 ± 1	152 ± 6	96 ± 4	−57 ± 11	−123	30
2855	5.1	9.1	−22.4	1200 ± 1	16	50 ± 2	279 ± 1	449 ± 20	274 ± 13	−274 ± 13	−113	40
10 897	5.2	12.2	−19.5	1313 ± 1	15.5	35 ± 5	311 ± 2	151 ± 10	86 ± 24	−82.3 ± 14	−53	50
11 218	5.2	10.9	−21	1475 ± 2	19.7	60 ± 3	217 ± 3	373 ± 6	199 ± 7	−184 ± 7	−90	50
11 283	7.8	13.4	−19	1954 ± 2	26	35 ± 10	281 ± 2	408 ± 17	235 ± 5	+178 ± 18	+32	40
11 283c				2055 ± 2	27.4	60 ± 5	134 ± 2	53 ± 3	44 ± 1	+24 ± 1	+50	40
11 300	6.4	11.9		467 ± 1	6.3	65 ± 10	344 ± 1	219 ± 34	123 ± 11	−110 ± 13	−78	50
11 891	9.9	13.6	−19.7	495 ± 3	6.1	40 ± 5	314 ± 3	174 ± 10	97 ± 4	−84 ± 7	−97	60
11 951	1.1	12.2	−20	1078 ± 2	14	65 ± 5	39 ± 3	409 ± 8	205 ± 8	+205 ± 8	+86	40
12 212	8.8			886 ± 2	11.8	55 ± 5	249 ± 2	57 ± 4	54 ± 18	+47 ± 4	+51	70

radius, we consider elliptical rings with a width of 3 to 6 pixels (∼3″ to 6″) and we thus obtain a middle velocity and radius for each ring. The choice of the width of the rings depends on the quality of the data and on the extension and slope of the rotation curve. Note that, for the barred galaxies of our sample (7/15), we have plotted a rotation curve including the perturbations induced by the bar because of non-circular motions along the bar.

4. Comments on the observed galaxies

UGC 528

This SAB(rs)b galaxy has a very compact spiral structure. There is Hα emission all over the optical disk which shows a barred spiral structure. The isovelocity map confirms the presence of a bar and suggests a warp (independently of the bar) in the outer parts of the optical disk. As a result, the major axis is not quite perpendicular to the minor axis (100° between the two), but the rotation curve remains symmetric and regular until 30 arcsec (3 kpc) with a maximum of 75 km s^{-1} at 16 arcsec, then rises because of the warped disk. The velocity amplitude is very faint for such a galaxy, for which the expected value is generally much higher. On the other end, the HI velocity field provided by WHISP is completely disturbed, with no clear velocity gradient at large scale although a gradient can be seen at smaller scales with a major axis of ≃290°, completely different (≃70°) from that derived by GHASP.

UGC 1249

This SB(s)m galaxy exhibits an asymmetric structure on the DSS image also observed on the Hα emission, which is mainly localized in what looks like a central bar and on the north-west side, suggesting a distorted spiral arm. No clear nucleus was detected on the continuum map and the center of rotation was chosen in order to derive the most regular and symmetric rotation curve possible. This rotation curve is quite chaotic but it seems that (from the approaching side) we reach a plateau at 70 km s^{-1} beyond 130 arcsec (2.8 kpc). About 9 arcmin to the north-east, UGC 1249 has a

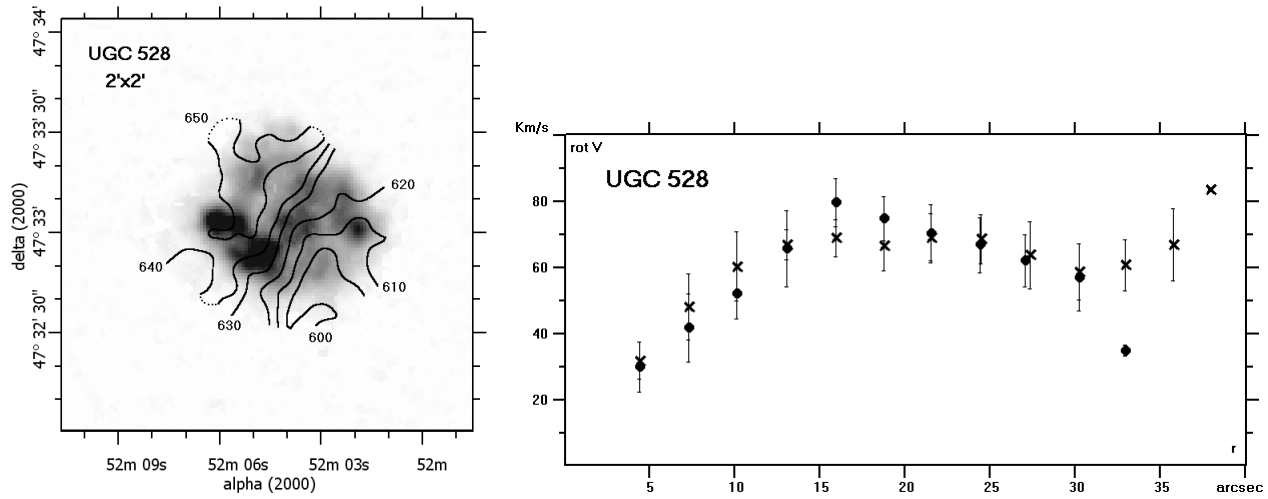

Fig. 1. UGC 528. At left: GHASP monochromatic image with Hα radial velocities superposed. At right: Hα rotation curve (crosses for receding side and dots for approaching). The field of view is 2 square arcminutes.

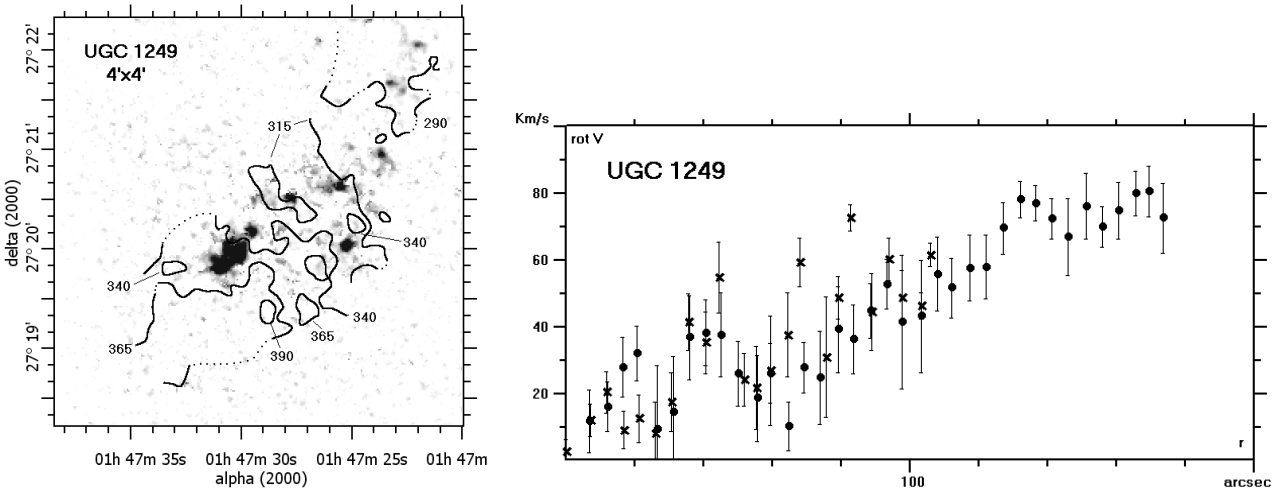

Fig. 2. UGC 1249. At left: GHASP monochromatic image with Hα radial velocities superposed. At right: Hα rotation curve (crosses for receding side and dots for approaching).

companion, UGC 1256, with which it seems to be interacting. Indeed, on the HI map derived by WHISP, one can see that their HI disks are contiguous and their velocity fields are regular and show a continuity in the isovelocity lines. The amplitude of the HI velocity field is in agreement with that derived by GHASP, confirming that we reach a plateau on the approaching side.

UGC 1256

In this SB(s)cd spiral companion of UGC 1249, the HII regions are arranged along a bar in the inner parts and seem to draw a weak spiral structure around it. For this late type galaxy, no clear nucleus can be seen on the continuum map which shows several knots in the central part. The rotation curve, like that of its neighbor UGC 1249, is irregular, notably in the inner parts where it shows a counter-rotation motion. Indeed, one can see an inversion of the sign of the velocities within 20 arcsec of the center, corresponding to two HII regions (that surrounded by the isovelocity 420 and that on its right), with a symmetric behaviour for both sides of the rotation curve. The center of rotation has been chosen in order to have the two sides of the rotation curve symmetrical, but we want to underline the fact that this peculiar motion of counter-rotation persists if we choose another knot as the center, showing that this motion is real. The curve begins to be fairly symmetric beyond 100 arcsec (3.9 kpc), seeming to reach a plateau around 80 km s^{-1}. However, according to the HI data, the plateau could be around 120 km s^{-1}. Unlike what Carozzi-Meysonnier (1982) claimed (namely that UGC 1256 was less affected by the interaction according to optical studies), it is hard to estimate which galaxy is the more perturbed. Concerning its content in atomic hydrogen, the WHISP data show that its column density is very high in the optical disk (more than 20×10^{20} atoms cm^{-2}), and that there is an extension of neutral gas to the north of the galaxy, which could be a tidal tail due to the interaction.

UGC 2023

This dwarf Im appears very diffuse on the optical image. The Hα emission is limited to some HII regions, mainly on the north-west side, as is often the case with this type of galaxy (see Van Zee 2000, about the Hα emission in dwarf galaxies). The rotation curve reaches the value of 60 km s^{-1} at 20 arcsec (note however the lack of information on the blueshifted side).

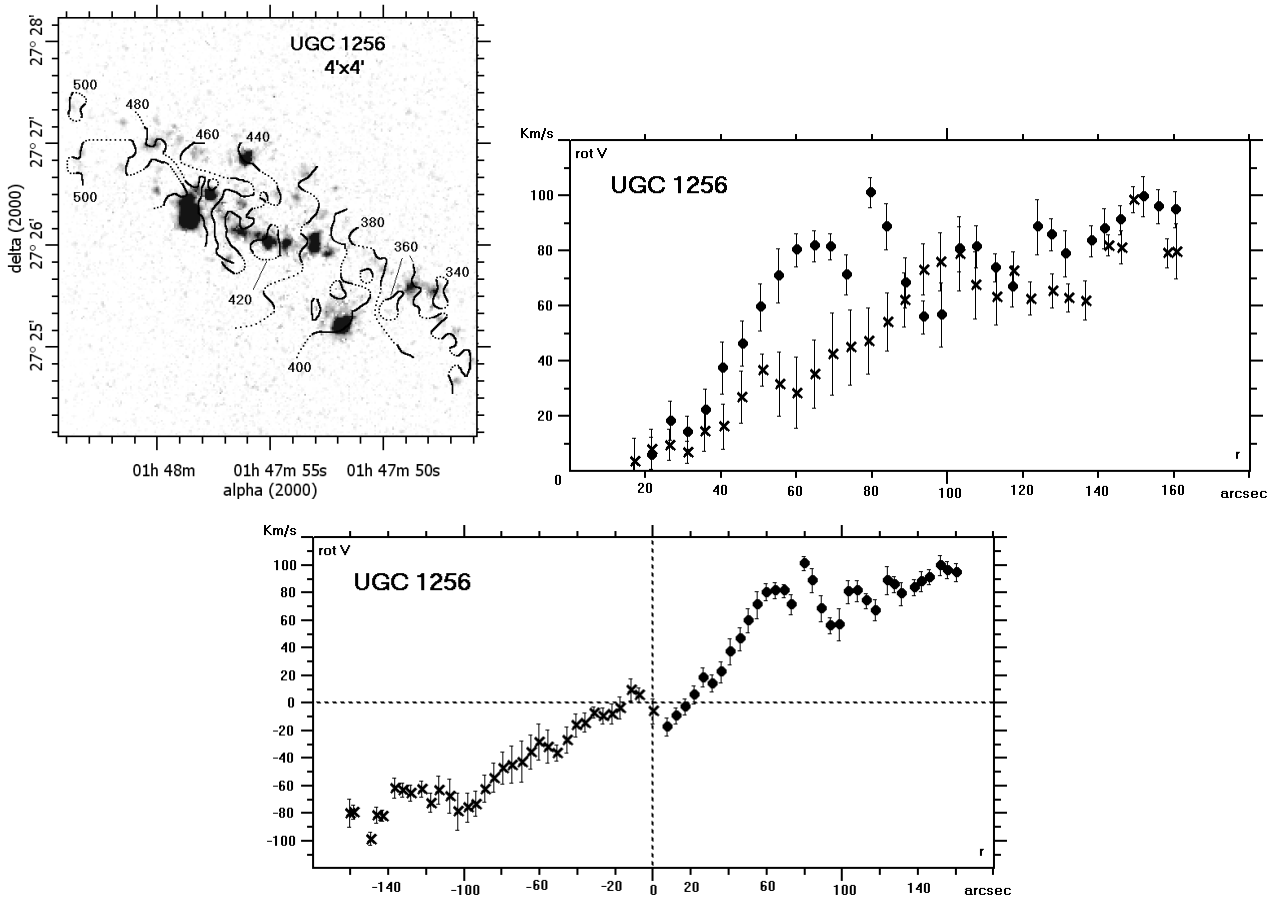

Fig. 3. UGC 1256. Top left: GHASP monochromatic image with Hα radial velocities superposed. Top right: Hα rotation curve (crosses for receding side and dots for approaching). Bottom: both sides of the rotation curve separated in order to show the anomalous motion in the center.

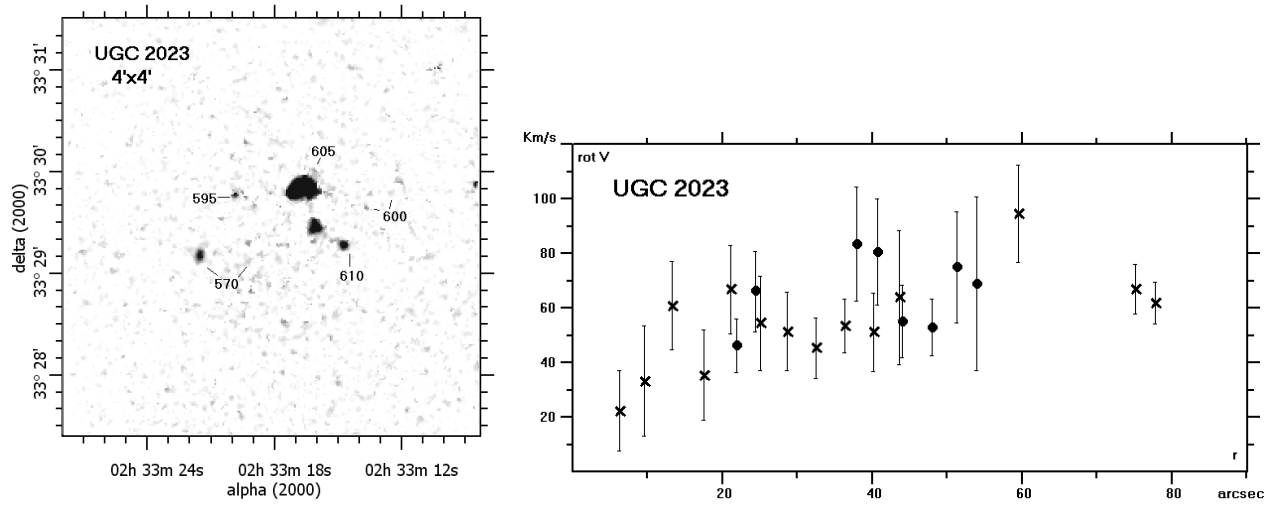

Fig. 4. UGC 2023. At left: GHASP monochromatic image with Hα radial velocities superposed. At right: Hα rotation curve (crosses for receding side and dots for approaching).

No nucleus was found and the kinematical center was determined in order to obtain the most symmetric rotation curve. The lack of emission makes it impossible to draw isovelocity lines. We have chosen the value of position angle for the major axis as determined by Swaters (1999). The spatial extension of the HI disk is the same as for the Hα emission. The rotation curve derived by Swaters is systematically lower by 20 km s^{-1} compared with that of GHASP and finally reaches the value of 60 km s^{-1} at 75 arcsec, whereas, in Hα, this value is already reached at 20 arcsec (0.8 kpc). However, the faintness of the HI signal and the large error bars of the Hα data make difficult to know which of Hα or HI is the most reliable to draw the rotation curve.

UGC 2053

This barred irregular galaxy has Hα emission only in its very central parts. No rotation curve could be derived because of the scarcity of Hα information. According to the velocity field provided by WHISP, the Hα emission is located along the minor axis, explaining why the faint Hα velocity gradient does not match the HI rotation curve. For these regions, nevertheless, our velocity values are in agreement with the WHISP ones. On the HI velocity field, one can note the alignment of the isovelocities along the photometric major axis of the galaxy, characteristic of the velocity perturbations induced by a bar. The rotation curve derived by Swaters (1999) is regular and increases until it reaches 100 km s^{-1} at 60 arcsec.

UGC 2082

This edge-on galaxy presents HII regions all over its optical disk. The rotation curve is fairly symmetric and seems to reach a plateau at 70 km s^{-1} (although the velocity dispersion is large). Note that the large error bars (≃60 km s^{-1}) are more found on the receding side beyond 60 arcsec. Despite the strong inclination of this galaxy, an isovelocity map could be derived. There is a good agreement with the HI data (WHISP) which show the same velocity amplitude.

UGC 2855

In this bright SABc spiral, the distribution of the ionized gas is much stronger on the north-west side (we retrieve this difference on the optical image). The isovelocity lines are symmetric with respect to the minor and major axis. The solid-body part of the rotation curve reaches 200 km s^{-1} at a radius of 35 arcsec (2.7 kpc); the rotation curve remains symmetric until 60 arcsec, then the blueshifted side (where Hα shows the most important emission) rises and separates from the redshifted one that remains flat around 200 km s^{-1}, underlining a possible warp of its disk on one side. Indeed, the velocity field derived by WHISP clearly shows a warp on the north-west side beyond the optical limit probably caused by the vicinity of its companion, UGC 2866 at 10 arcmin (≃90 kpc). The same remark can be made for the disk of UGC 2866 which is warped. The star formation, mainly localized in the west arm, together with the asymmetry of the rotation curve and the disturbed HI disks of the two galaxies, clearly suggests that they are interacting. The position-velocity diagram in the CO line emission derived by Sofue et al. (1997) shows that the rotation curve is flat after 30 arcsec, which is true if one considers the average of both sides.

UGC 10897

This almost face-on S(s)c spiral shows Hα emission in its bulge and all along its spiral arms. Its rotation curve is symmetric but with large velocities dispersion (40 km s^{-1} in average) due to the small inclination and marks a plateau at 70 km s^{-1} (note that the fall of the blueshifted velocities is linked to the beginning of the north-west arm). The position angle of the major axis (290°) has been chosen with the help of the velocity field of WHISP because the position angle deduced at first glance by the Hα velocity field (≃311°) produces a rising rotation curve which goes beyond 110 km s^{-1}, never reaching a plateau. Also, the HI data suggest that the maximum of the rotation curve is reached within the optical limit of the disk, with a velocity amplitude rather faint for such a galaxy for which the expected value is generally much higher.

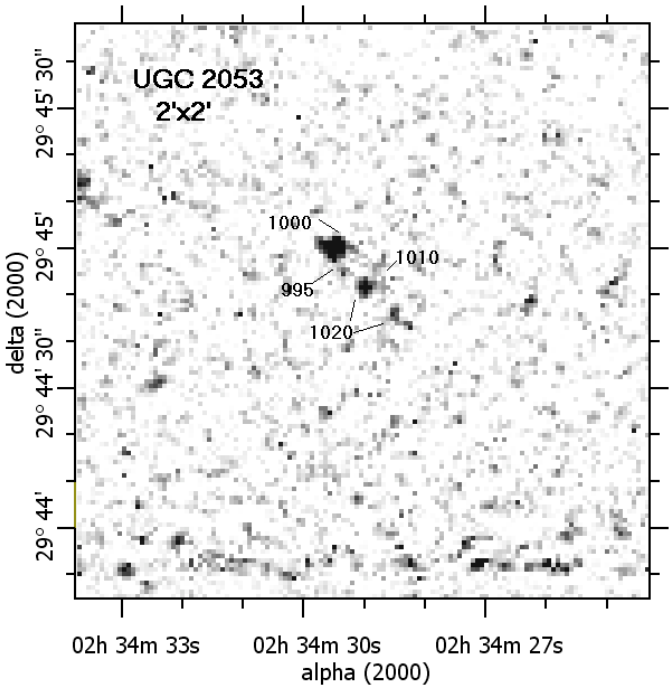

Fig. 5. UGC 2053. GHASP monochromatic image with Hα velocities superposed. No Hα rotation curve could be derived. The field of view is 2 square arcminutes.

UGC 11218

This S(rs)b galaxy is rich in ionized gas. The Hα map clearly shows the spiral structure. The rotation curve is perfectly regular and symmetric, reaching a plateau around 180 km s^{-1} at 30 arcsec (2.9 kpc). The isovelocity map exhibits distortions when crossing the arms and also a strong gradient in the inner parts. The whole optical disk is very rich in neutral gas according to the HI map provided by WHISP. The HI velocities are in good agreement with the Hα ones.

UGC 11283

This Magellanic galaxy exhibits a barred spiral structure with two arms showing different behaviours. There is Hα emission in the bulge and the two arms, with an extension for the north arm. The isovelocities map underlines the presence of the bar through the peculiar direction taken by the lines. The rotation curve is of solid-body type for the approaching side and reaches a plateau around 180 km s^{-1} at 20 arcsec (2.5 kpc) for the receding side. The velocity amplitude is rather high for such a galaxy. The HI data suggest that the maximum is reached within the optical limit of the galaxy but show no distorsions of the isovelocities at the bar, certainly because of the beam-smearing. Note the presence of an isolated cloud of neutral hydrogen, possibly in orbit around UGC 11283.

UGC 11283 companion

This barred dwarf galaxy is localized at 5.9 arcmin north of UGC 11283. Optically, it appears as an irregular galaxy, and its Hα emission consists of a few HII regions. The rotation curve is ill-defined and, in order to draw it, the center of rotation, major axis and inclination have been determined from the

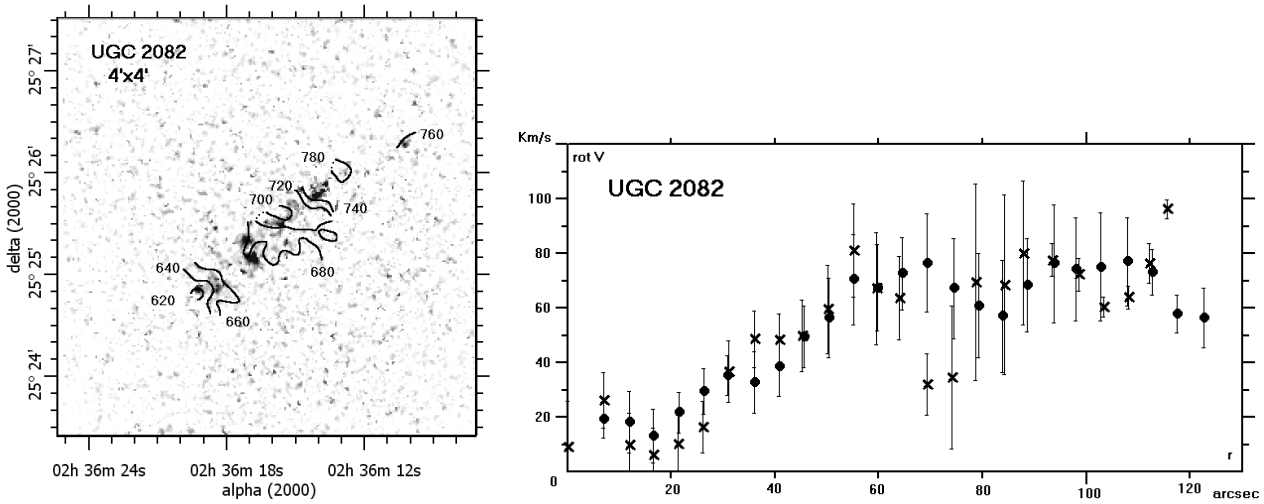

Fig. 6. UGC 2082. At left: GHASP monochromatic image with Hα velocities superposed. At right: Hα rotation curve (crosses for receding side and dots for approaching).

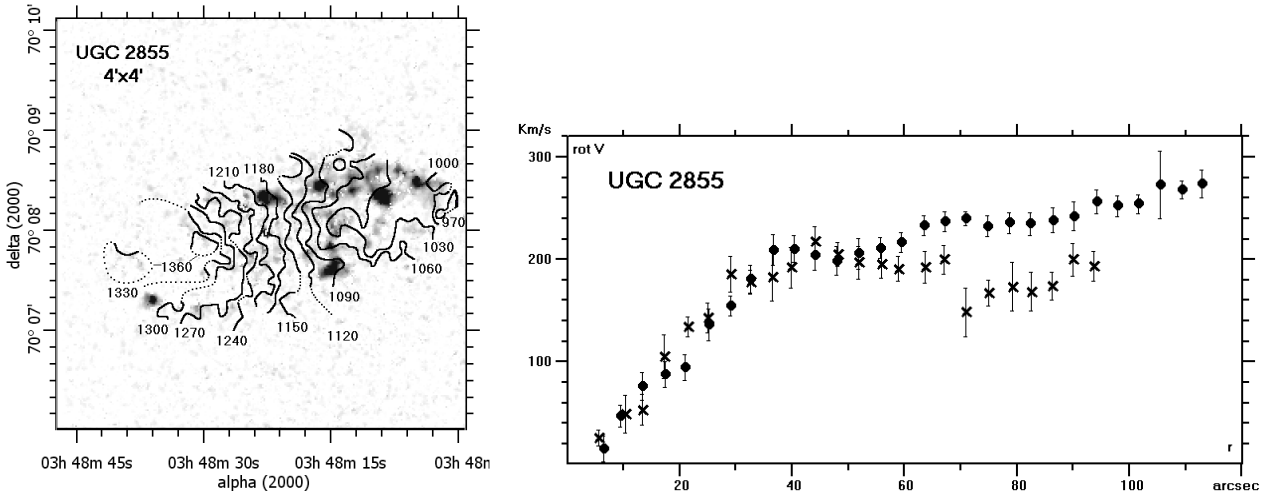

Fig. 7. UGC 2855. At left: GHASP monochromatic image with Hα velocities superposed. At right: Hα rotation curve (crosses for receding side and dots for approaching).

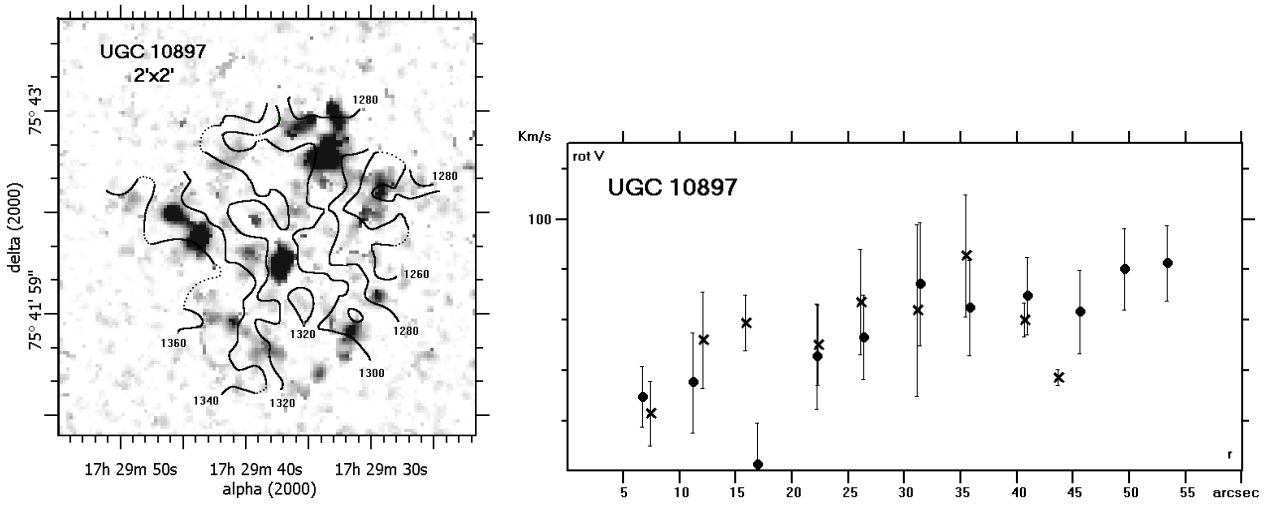

Fig. 8. UGC 10897. At left: GHASP monochromatic image with Hα radial velocities superposed. At right: Hα rotation curve (crosses for receding side and dots for approaching). Note that the field of view is 2 square arcminutes.

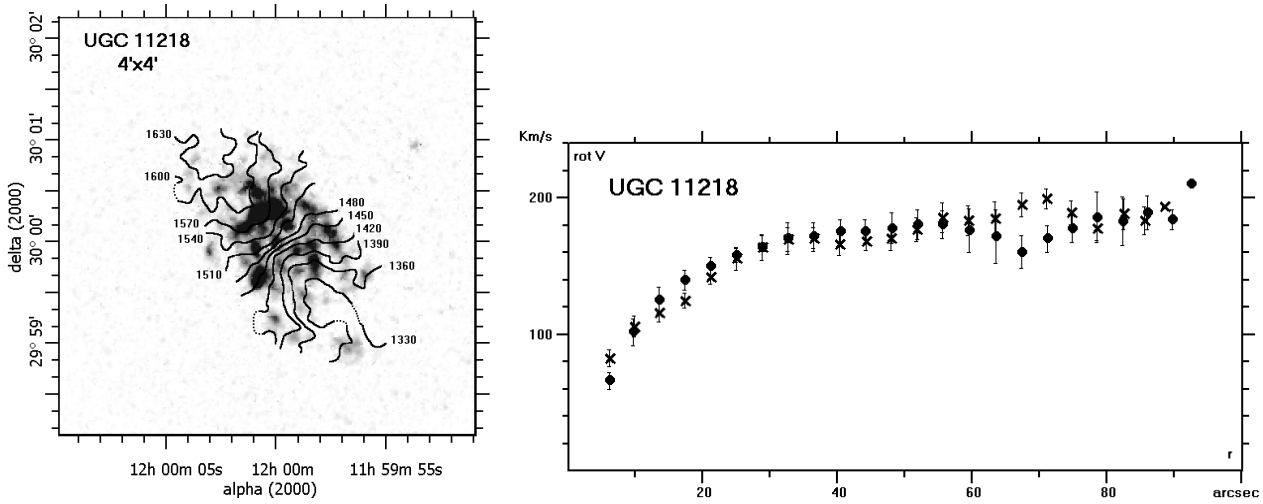

Fig. 9. UGC 11218. At left: GHASP monochromatic image with Hα radial velocities superposed. At right: Hα rotation curve (crosses for receding side and dots for approaching). Note that the field of view is 2 square arcminutes.

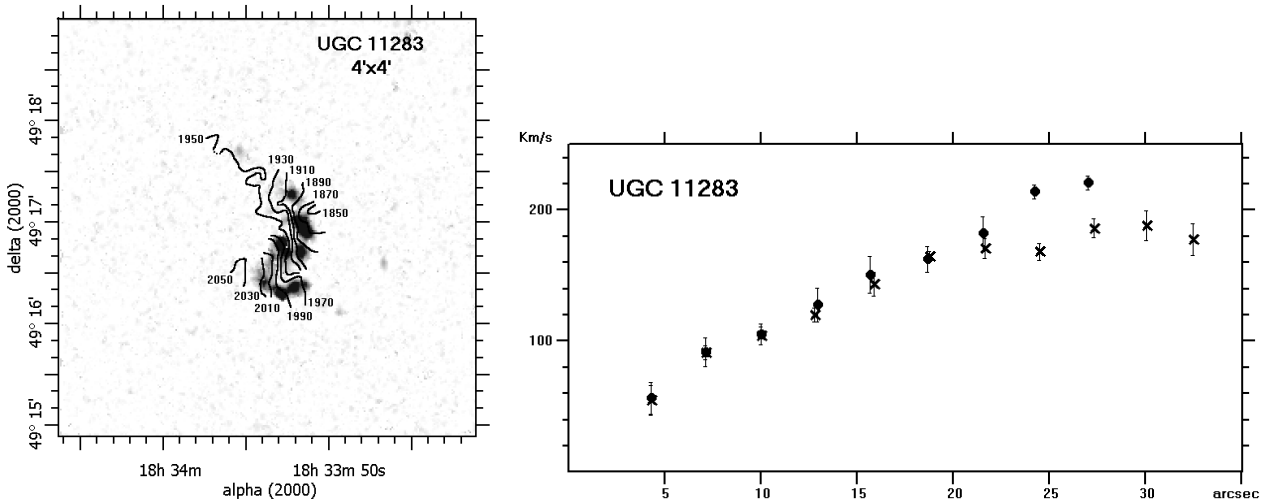

Fig. 10. UGC 11283. At left: GHASP monochromatic image with Hα radial velocities superposed. At right: Hα rotation curve (crosses for receding side and dots for approaching).

regular HI velocity field of WHISP which displays the same faint radial velocity amplitude.

UGC 11300

This galaxy is highly inclined and exhibits bright HII regions with fainter Hα emission on the north side because of the filter which cuts out the lowest velocities. There is an elongated bulge which appears on the continuum map but no clearly marked nucleus. Both sides of the rotation curve behave differently: the redshifted side has a solid body rotation curve, whereas the blueshifted side exhibits a plateau around 35 km s^{-1} up to 40 arcsec, then it increases again without ever reaching the redshifted side. There is no companion in the vicinity that could explain such an asymmetry in the rotation curve. Also, the WHISP data show that the HI disk is strongly warped in its outer parts, suggesting again a perturbation by an unseen companion. They suggest too that the maximum is reached by the receding side.

UGC 11891

This galaxy, with low surface brightness on the optical image, presents very faint Hα emission with some disseminated HII regions. The derived rotation curve is not reliable because of the small number of velocity points and cannot be drawn in the central part because of the lack of HII regions there. The low rotation velocities found on the redshifted side, around 50 arcsec, come from the two HII regions with radial velocity 505 km s^{-1} on the velocity map. The value 100 km s^{-1} reached by the blueshifted side seems to be the maximum of the rotation curve according to the WHISP data. The inclination and major axis we have adopted are those given by WHISP since the HI velocity field is well defined. Note that the HI data suggest a warp of the outer parts of the HI disk.

UGC 11951

This galaxy has a bar with strong Hα emission and there are bright HII regions in the west spiral arm whereas there is only faint diffuse Hα emission on the east side where no spiral arm

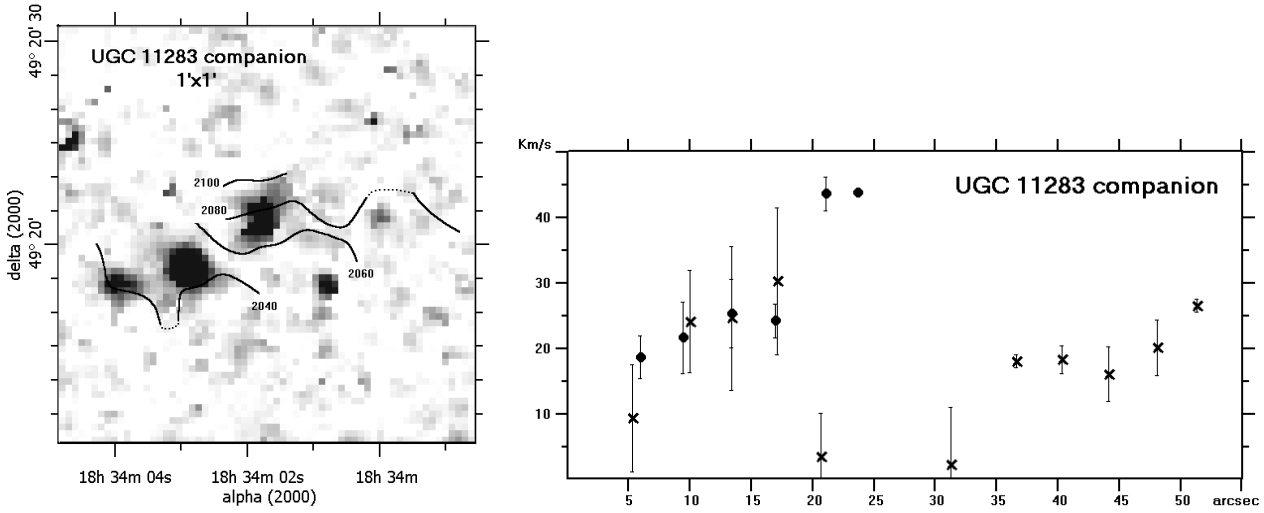

Fig. 11. UGC 11283 companion. At left: GHASP monochromatic image with Hα radial velocities superposed. At right: Hα rotation curve (crosses for receding side and dots for approaching). In this case, the field of view of the images is 1 square arcminute.

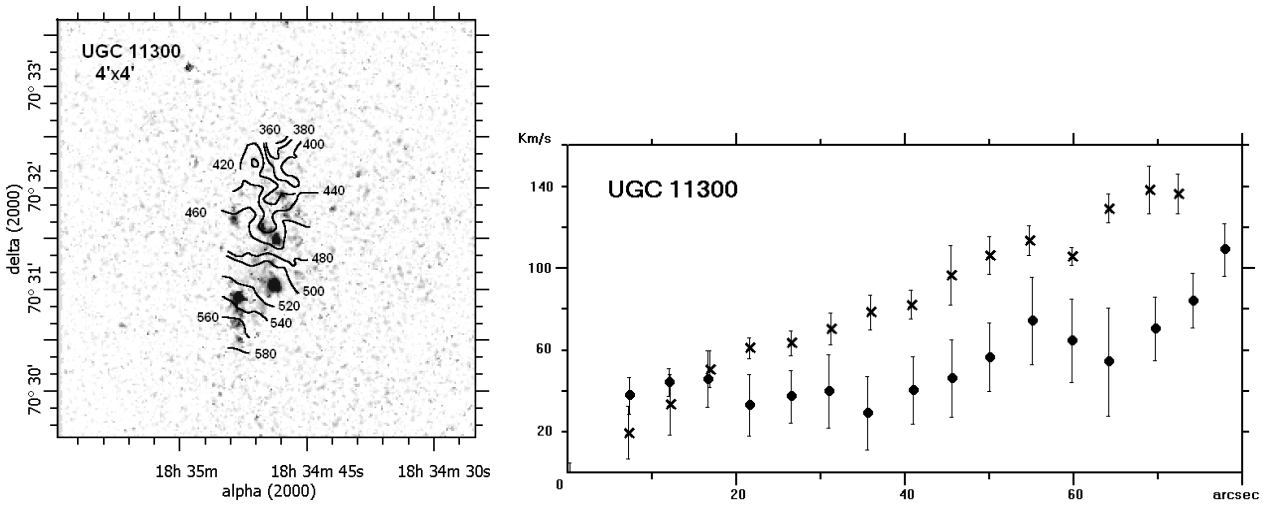

Fig. 12. UGC 11300. At left: GHASP monochromatic image with Hα radial velocities superposed. At right: Hα rotation curve (crosses for receding side and dots for approaching).

can be seen on the optical image. The isovelocity lines design suggests a warp in the outer parts (confirmed by the HI velocity field), well marked on the blueshifted side, and shows the classical S-shaped distortions produced by a bar in the central part. The value adopted for the position angle of the major axis is that suggested by the WHISP data for the outer parts. The resulting rotation curve is fairly symmetric and shows a solid body rotation curve. This behaviour is in agreement with the HI data showing that the plateau is barely reached at 2 arcmin from the center (see position-velocity plot), but comparing our radial velocities with that of WHISP, suggest that the maximum is just reached at the end of the Hα curve.

UGC 12212

This irregular galaxy has a few bright HII regions scattered all over its disk as can be seen also on the Hα image by Van Zee (2002). It is almost impossible to draw the velocity field and we just plotted the radial velocities of the main regions. The rotation curve has large error bars and suggests that a plateau is reached around 40 km s^{-1} at about 20 arcsec, up to our outermost Hα velocity points at 1 arcmin. However, the position-velocity plot derived by WHISP shows that the rotation curve is of a solid-body type all along the optical disk and beyond, up to the HI limit.

5. Discussion

We could derive a fairly regular and symmetric rotation curve for 8 galaxies (UGC 528, UGC 1256, UGC 2082, UGC 2855, UGC 10897, UGC 11218, UGC 11283, UGC 11951) with morphological types earlier than $t = 8 \equiv$ Sd. We have obtained three rotation curves of solid-body type for UGC 1249, UGC 11283, UGC 11951. These galaxies present some peculiarities: UGC 1249 is interacting with its companion UGC 1256; UGC 11283, strongly barred, has a companion at 5.9 arcmin and a cloud of neutral hydrogen is in orbit around it; UGC1 1951, also barred, presents a warped disk in optic

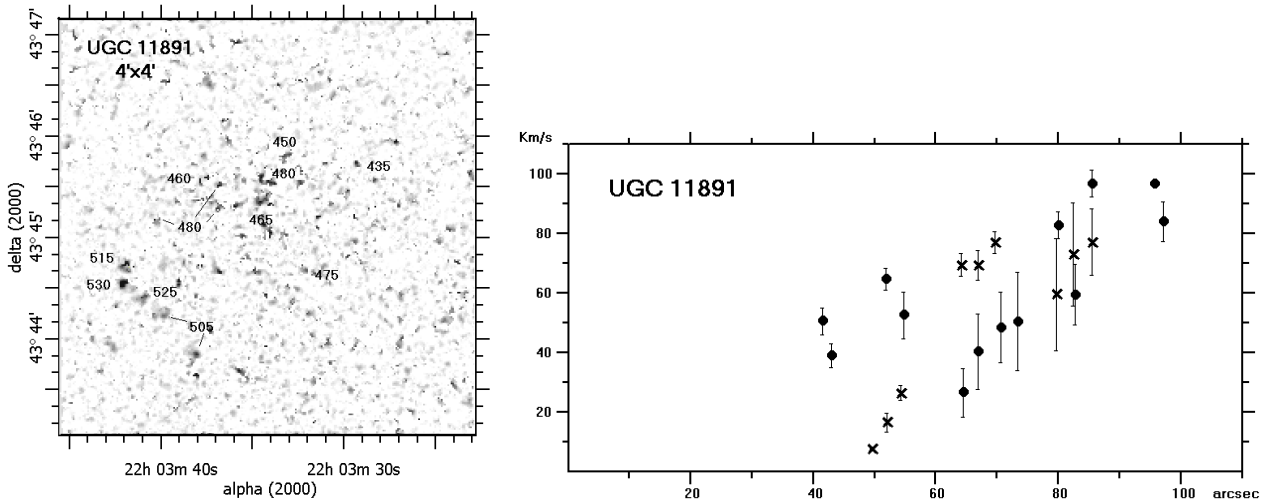

Fig. 13. UGC 11891. At left: GHASP monochromatic image with Hα radial velocities superposed. At right: Hα rotation curve (crosses for receding side and dots for approaching).

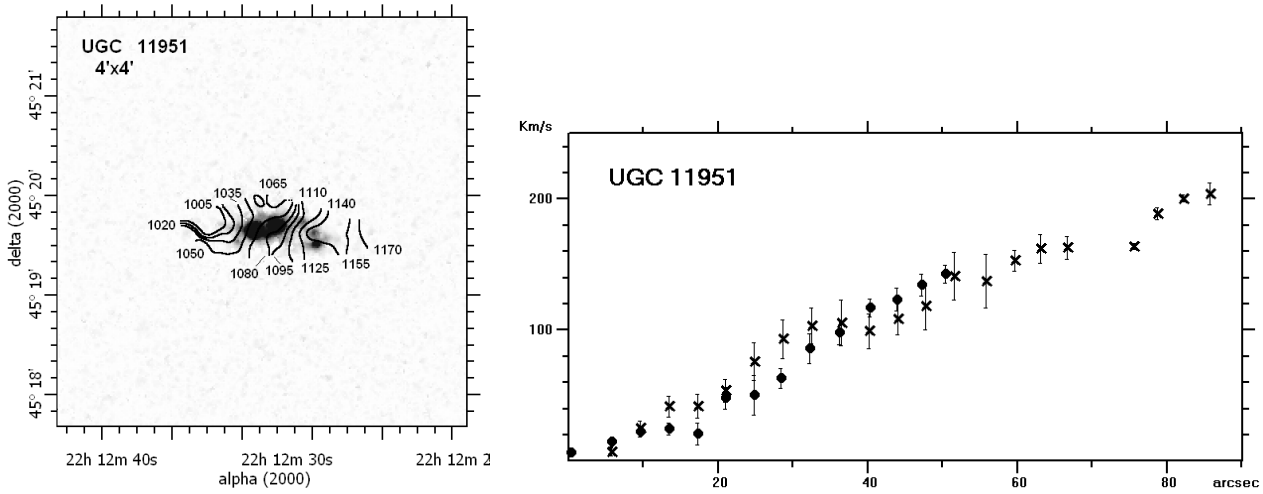

Fig. 14. UGC 11951. At left: GHASP monochromatic image with Hα radial velocities superposed. At right: Hα rotation curve (crosses for receding side and dots for approaching).

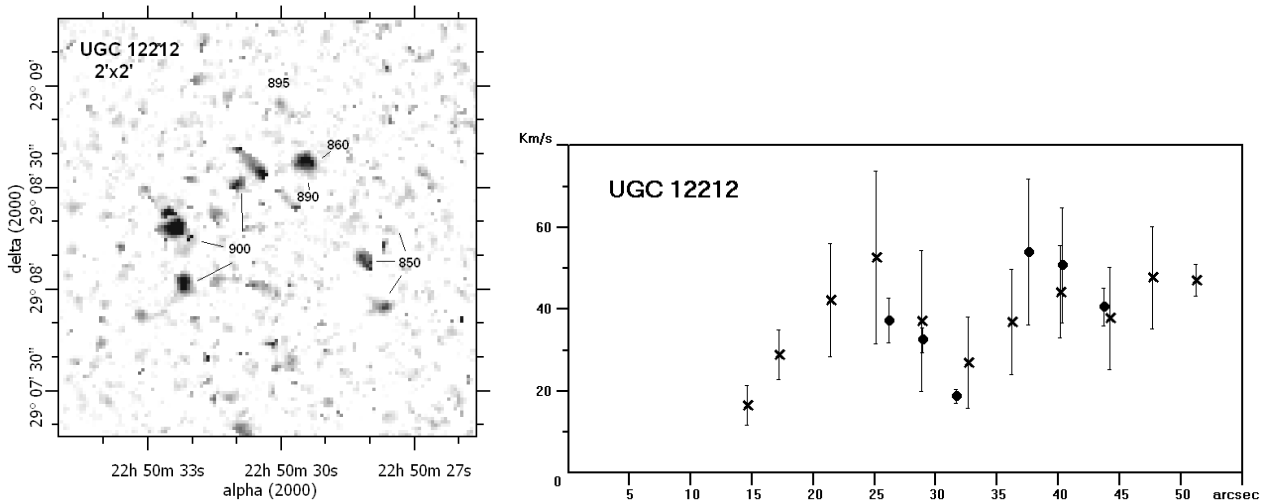

Fig. 15. UGC 12212. At left: GHASP monochromatic image with Hα radial velocities superposed. At right: Hα rotation curve (crosses for receding side and dots for approaching). Note that the field of view is 2 square arcminutes.

(confirmed in radio) suggesting that it has suffered from an interaction in the past. The five galaxies with irregular rotation curves are very late-type galaxies with $t \geq 8.8$. Three of them have a faint Hα emission with only a few HII regions without any diffuse emission. UGC 11300 is a peculiar case, with quite different behaviors on both sides. For one galaxy, UGC 2053, no rotation curve could be derived because of the lack of Hα emission; and for another one, UGC 1249, a counter-rotation motion has been detected. Peculiar motions in the central parts due to the presence of a bar have been detected for 3 galaxies: UGC 528, UGC 11283 and UGC 11951.

The five galaxies with very late-type ($t \geq 8$) studied here display irregular rotation curves. However, no systematic conclusion may be adopted at this stage since, in Paper I, only 4 out of 11 had irregular rotation curves. Looking at our sample in its present stage, it is clear that only very late-type galaxies exhibit an irregular rotation curve (excluding the cases of interacting galaxies for which earlier types of galaxies are likely also to exhibit disturbed rotation curves).

As mentioned in Sect. 1, the largest sample of optical data cube of nearby and isolated spirals found in the literature is that of Schommer et al. (1993) with 75 galaxies. The GHASP survey will provide an unique 2D sample of about 200 galaxies in the Hα line, using a Fabry-Perot interferometer. Thanks to this survey, a 2D reference sample will be built in order to make comparisons with galaxies in various environments (pairs, groups, clusters) or at different stages of their evolution (mergers, starbursts, galaxies at higher redshifts). In this paper, we have presented a new set of 15 galaxies; further data will be presented in forthcoming papers. The data reduction is in progress and a more complete analysis of the 2D velocity fields will be made in subsequent papers, including: comparison between HI and Hα velocity fields; study of non-circular motion (e.g. effect of the bar, counter-rotation motion...); derivation of the Tully-Fisher relation, study of the luminous and dark matter distribution (Amram & Garrido 2002) and study of internal kinematics using simulations (hierarchical N-BODY code coupled to hydrodynamical SPH code).

Acknowledgements. The authors thank the Groupement de Recherche Galaxies for its support for observing time and the Observatoire de Haute-Provence team for its technical assistance during the observations. They also thank the referee Dr N. Devereux who helped improve the manuscript. This research has made use of the NASA/IPAC Extragalactic Database (NED) which is operated by the Jet Propulsion Laboratory, California Institute of Technology, under contract with the National Aeronautics and Space Administration. We have also made use of the LEDA database (`http://leda.univ-lyon1.fr`).

References

Amram, P., & Garrido, O. 2002, Galaxies: the third dimension, ed. M. Rosado, L. Binette, & L. Arias [`astro-ph/0202475`]
Beauvais, C., & Bothun, G. 2001, ApJS, 136, 41
Carozzi-Meyssonnier, N. 1982, A&AS, 47, 237
Garcia-Barreto, J. A., & Rosado, M. 2001, AJ, 121, 2540
Garrido, O., Marcelin, M., Amram, P., & Boulesteix, J. 2002, A&A, 387, 821
Gavazzi, G., Marcelin, M., Boselli, A., et al. 2001, A&A, 377, 745
Mendes de Oliveira, C., Plana, H., Amram, P., Balkowski, C., & Bolte, M. 2001, AJ, 121, 2524
Östlin, G., Amram, P., Bergvall, N., Masegosa, J., Boulesteix, J., & Márquez, I. 2001, A&A, 374, 800
Östlin, G., Amram, P., Masegosa, J., Bergvall, N., & Boulesteix, J. 1999, A&AS, 137, 419
Palunas, P., & Williaùs, T. B. 2000, AJ, 120, 2884
Plana, H., Amram P., Mendes de Oliveira, C., & Balkowski, C. 2000, AJ, 120, 621
Rozas, M., Relano, M., Zurita, A., & Beckman, J. E. 2002, A&A, 386, 42
Schommer, R. A., Bothun, G. D., Williams, T. B., & Mould, J. R. 1993, AJ, 105, 97
Sofue, Y., Tutui, Y., Honma, M., & Tomita, A. 1997, AJ, 114, 2428
Swaters, R. A. 1999, Dark matter in late-type dwarf galaxies, Thesis, Rijksuniversiteit, `Groningen.http://www.ub.rug.nl/eldoc/dis/science/r.a.swaters/`
Van Zee, L. 2000, AJ, 119, 2757
de Vaucouleurs, G. 1979, ApJ, 227, 380